Cross-Stream Migration of Driven Polymer Solutions in Nanoscale Channels: A Numerical Study with Generalized Dissipative Particle Dynamics

Jaime A. Millan[†] **and Mohamed Laradji***[,‡]

Department of Physics, The University of Memphis, Memphis, Tennessee 38152-3390, and MEMPHYS−Center for Biomembrane Physics, University of Southern Denmark, Odense, DK-5230, Denmark

Received June 27, 2008; Revised Manuscript Received December 2, 2008

ABSTRACT: Polymer solutions in nanoscale slit pores and undergoing uniform pressure gradient (Poiseuille) flow are investigated via generalized dissipative particle dynamics simulations. In particular, the trend of cross-stream migration of the polymer chains during flow is investigated as a function of Schmidt number through varying the strength of the two-body dissipative and random forces in the dissipative particle dynamics formalism. For a given polymer solution, a migration away from the walls is observed as Schmidt number is increased. For a given Schmidt number, a migration away from the walls is also observed with increasing the driving force for relatively short chains. However, for long chains, a migration toward the walls is observed with increasing the driving force. We also analyzed the effects of channel thickness and temperature on the trend of the cross-stream migration of the polymer chains.

1. Introduction

Fluids that are confined in microscale or nanoscale geometries may exhibit structural and transport properties that are different from those of nonconfined fluids.[1] In particular, the structure and transport properties of polymer solutions are altered when the polymer radius of gyration is comparable to the characteristic length scale of the confining geometry.[2−6] The understanding of transport properties and structure of confined fluid solutions containing polymers, including biopolymers such as DNA and proteins, in nanoscale or microscale channels, is crucial to a variety of applications such as sequencing of DNA molecules, electrophoresis, DNA translocation through transmembrane protein pores, adhesion, lubrication, chromatography, polymer processing, and oil recovery. Recent advances made in the field of nanofluidics underlines the importance of studying the transport properties of polymer solutions in nanoscale channels.[7−10]

A polymer solution undergoing steady state flow, such as Couette or Poiseuille flow, or oscillatory shear flow, experiences shear forces which lead to the elongation of the polymer chains along the flow direction. Experiments reported a net cross-stream migration of the polymer chains toward the channel's middle,[7,11−13] leading to a concentration profile that is distorted from that of the solution at equilibrium. Earlier thermodynamic arguments suggest that the migration of the polymer chains, in the case of Poiseuille flow, is due to the fact that shear-gradient is lowest at the centerline, and therefore higher chain entropy in the centerline region. Meanwhile, due to the stretching of the polymer chains in shear flow, the entropic exclusion near the wall is reduced, and therefore thermodynamic arguments would also predict a decrease in the depletion layer near the walls. The thermodynamic arguments predict that in the case of uniform shear flow (Couette), the polymer mass distribution away from the walls should be uniform. In contrast, a migration away from the walls is also observed in Couette flow. Consequently, polymer migration away from the walls is due to the combined effects of hydrodynamics, finite shear rate, and the presence of confining walls, and cannot simply be accounted for by thermodynamic arguments.

An early kinetic theory of an elastic dumbbell near a wall, by Jhon and Freed,[14] with an approximate wall-dumbbell hydrodynamic interaction, found a migration of the dumbbell away from the wall. A recent and more refined kinetic theory by Jendrejack et al.[15] and Ma and Graham[16] predicts that the direction of migration, of an elastic dumbbell in vicinity of a wall and undergoing Poiseuille flow, depends on whether the wall-dumbbell hydrodynamic interaction is accounted for or not. In particular, if bulk hydrodynamics are accounted for while the wall-hydrodynamic interaction is ignored, a migration toward the wall is observed.[15] In contrast, if the wall-dumbbell hydrodynamic interaction is accounted for in addition to bulk hydrodynamics, a migration to the channel centerline is observed. The migration of the polymer chains toward the centerline is countered by the chains thermal diffusion. In the case of Poiseuille flow, the polymer conformations become anisotropic due to their stretching along the channel. However, due to the gradient in shear rate, the degree of conformational anisotropy is higher near the walls than in the centerline region. As a result, the chains diffusivity across the channel is nonuniform. This leads to two off-center peaks in the cross-stream polymer distribution. In contrast, the degree of anisotropy is uniform across the channel in the case of Couette flow, leading to a polymer distribution with a single peak at the centerline of the channel.

Various numerical approaches were recently employed to investigate dilute polymer solutions in Poiseuille flow or Couette flow. These include (i) Brownian dynamics woth fluctuating hydrodynamic interactions (BDHI) approach where the solvent is treated implicitly as a continuum medium while the polymer chains are represented by linear sequences of beads, and the interbead hydrodynamic interactions are treated using the Stokeslet formalism,[15,17−23] (ii) lattice Boltzmann dynamics (LBD),[24−27] (iii) molecular dynamics (MD),[29] and (iv) dissipative particle dynamics (DPD).[30−32] Both BDHI and LBD simulations have extensively been used particularly in studying the transport of DNA molecules in nanoscale or micronscale slit pores and undergoing Poiseuille or Couette flow. A detailed

* Corresponding author. E-mail: mlaradji@memphis.edu
[†] Department of Physics, The University of Memphis.
[‡] MEMPHYS−Center for Biomembrane Physics, University of Southern Denmark.

10.1021/ma8014382 CCC: $40.75
Published on Web 01/15/2009

comparison between BDHI and LBD was recently performed.[28] Although a cross-stream migration away from the walls was predicted by both approaches, the details of the polymer density profiles were different in the two approaches. These differences were attributed to artifacts in both methods, namely the use of a discrete lattice in LBD and lack of inertial effects in BDHI. While BDHI, LBD and MD simulations seem to predict a migration of the polymer chains toward the centerline of the channel, in agreement with the kinetic theory, results of the DPD simulations have been rather inconclusive. In particular, in our recent DPD simulations of a dilute and semidilute polymer solution,[31] a migration toward the walls was observed for long polymer chains. However, a migration weaker than that observed previously with LBD and BD was observed for relatively short polymer chains. In the more recent DPD simulations of Fedosov et al., a migration toward the walls was observed.[32]

Fluids, modeled via conventional DPD[33] exhibit very low viscosity, and are thus characterized by a Schmidt number (defined as the ratio between the speed of momentum transfer and that of mass transfer) which is much smaller than that of a regular fluid such as water. In a fluid with low Schmidt number, the velocity field may not be fully developed during the kinetics of polymer chains, leading to a suppression of the hydrodynamic interaction between the polymeric monomers and the wall, which is believed to be responsible for driving the polymer chains away from the walls. We are therefore faced with the problem that while BDHI, LBD and MD are able to correctly predict a polymer migration away from the walls in Poiseuille or Couette flow, the DPD approach, which has been shown through a large number of studies to faithfully describe the kinetics in various complex fluids, is not in full agreement with experiments and the kinetic theory. In order to elucidate this apparent discrepancy, we carried out a systematic set of simulations using a generalized DPD approach with modified random and dissipative forces, recently developed by Fan et al.,[34] that allows for varying the Schmidt number by a factor more than 10 for a given set of conservative interactions.

2. Model and Method

As mentioned above, the transport of polymer solutions in planar slits and in the presence of uniform pressure gradient is investigated using the dissipative particle dynamics (DPD) approach.[35−37] Although DPD is reminiscent of molecular dynamics, it uses soft repulsive interactions, thereby allowing for larger integration time increments than in a typical molecular dynamics using Lennard-Jones interactions. In the present study, solvent particles and polymer chains are confined between two planar plates along the *xy*-plane. Solvent (*s*), polymer (*p*), and wall (*w*) particles are all soft DPD-particles. The wall particles are considered to be static, arranged in a face-centered-cubic lattice, with a number density higher than that of the fluid in order to ensure the impermeability of the wall. DPD also uses pairwise random and dissipative forces between neighboring particles, which are interrelated through the fluctuation−dissipation theorem. The pairwise nature of these forces ensures that momentum is locally conserved, a necessary condition for correct long-range hydrodynamics.[38,39] The equations of motion of a particle *i* are given by

$$\frac{\mathrm{d}}{\mathrm{d}t}r_i(t) = v_i(t) \tag{1}$$

$$\frac{\mathrm{d}}{\mathrm{d}t}v_i(t) = \frac{1}{m_i}\sum_j [F_{ij}^{(C)} + F_{ij}^{(D)} + F_{ij}^{(R)}] \tag{2}$$

(3)

where $F_{ij}^{(C)}$ is the two-body conservative force between particles *i* and *j* and as usual is soft, modeled by a linear form,

$$F_{ij}^{(C)} = \begin{cases} a_{ij}(1 - r_{ij}/r_c)\hat{r}_{ij} & \text{for } r_{ij} \le r_c \\ 0 & \text{for } r_{ij} > r_c \end{cases} \tag{4}$$

where $r_{ij} = r_j - r_i$ and $r_{ij} = r_{ij}/r_{ij}$. a_{ij} is the amplitude of the repulsive interaction between *i* and *j* and depends on their species. The values of the parameter a_{ij} are specifically chosen as

$$a_{ij} = \frac{\varepsilon}{r_c}\begin{pmatrix} & w & s & p \\ w & - & 3 & 10 \\ s & 3 & 25 & 25 \\ p & 10 & 25 & 50 \end{pmatrix} \tag{5}$$

where ε is the energy scale in the present simulation. Note that the interaction parameter a_{ww} is irrelevant since the wall particles are not allowed to move in the simulation. The importance of a_{ws} to the velocity field boundary condition will be discussed later. Note, as well, that in order to avoid adsorption of the polymer chains onto the wall, the interaction strength between the wall and the polymer particles is chosen to be more repulsive than that between the wall and solvent particles. The integrity of the polymer chains is ensured via an additional harmonic interaction between consecutive monomers,

$$F_{i,i+1}^{(S)} = -C(1 - r_{i,i+1}/b)\hat{r}_{i,i+1} \tag{6}$$

where we set $C = 100\varepsilon$ and $b = 0.45r_c$.

The specific value of the wall-solvent interaction, a_{ws}, combined with the wall number density, is important to the velocity field boundary condition.[31] Indeed for the used wall particles density, we found a slip boundary condition if $a_{ws} > 10\varepsilon/r_c$, with a slip length that increases with increasing a_{ws}. The present simulations are performed with $a_{ws} = 3.0\varepsilon/r_c$ for which a no-slip boundary condition in observed. As discussed in our previous article,[31] the velocity field of a simple DPD fluid is found to follow the quadratic Poiseuille−Hagen law when driven by a uniform pressure gradient, implying that the present DPD model is able to adequately model hydrodynamic flow.

The dissipative and random forces are given by

$$F_{ij}^{(D)} = \gamma\omega_D(r_{ij})(\hat{r}_{ij}\cdot v_{ij})\hat{r}_{ij} \tag{7}$$

$$F_{ij}^{(R)} = \sigma(\Delta t)^{1/2}\omega_R(r_{ij})\theta_{ij}\hat{r}_{ij} \tag{8}$$

where θ_{ij} is a symmetric random variable satisfying

$$\langle\theta_{ij}(t)\rangle = 0 \tag{9}$$

$$\langle\theta_{ij}(t)\theta_{kl}(t')\rangle = (\delta_{ik}\delta_{jl} + \delta_{il}\delta_{jk})\delta(t - t'), \tag{10}$$

and Δt is the time step in the simulation. The system is in a heat bath at some temperature *T*. The parameters γ and σ and weight functions, ω_D and ω_R, are therefore related to each other by the fluctuation−dissipation theorem

$$\gamma = \sigma^2/2k_BT, \tag{11}$$

$$\omega_D(r) = [\omega_R(r)]^2 \tag{12}$$

For the weight function ω_D appearing in eqs 7 and 12, we use a generalized form recently proposed by Fan et al.,[34]

$$\omega_D(r) = \begin{cases} (1 - r/r_c^{(D)})^q & \text{for } r \le r_c^{(D)} \\ 0 & \text{for } r > r_c^{(D)} \end{cases} \tag{13}$$

where $r_c^{(D)}$ is a cutoff distance for the dissipative and random forces, not necessarily equal to r_c. We note that in conventional DPD simulations, an exponent $q = 2$ is used.

Fan et al.[34] showed that this model leads to larger values of the viscosity of the fluid and smaller values of the self-diffusion coefficient, as the exponent *q* is decreased and/or the cutoff $r_c^{(D)}$

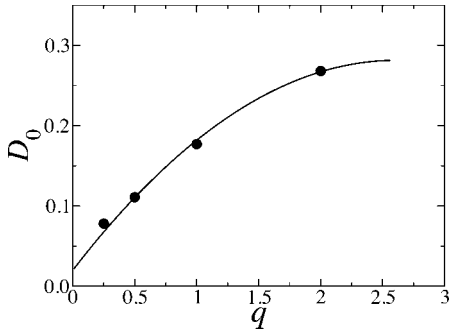

Figure 1. Self-diffusion coefficient vs the exponent, q, for a pure solvent. The solid line is only a guide for the eye.

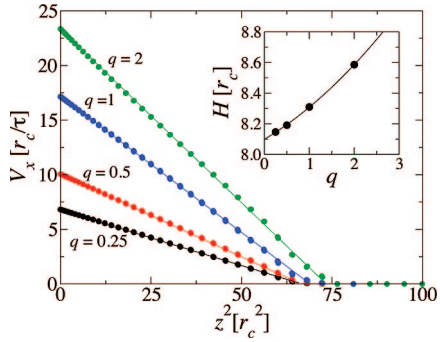

Figure 2. Solvent velocity profile in Poiseuille flow with $f_x = 0.2\varepsilon/r_c$. Data sets from top to bottom, at $z = 0$, correspond to $q = 2$, 1, 0.5, and 0.25, respectively. The solid lines are straight lines. The inset shows the effective slit thickness versus the exponent q. Note that as $s \rightarrow 0$, the slit thickness converges to $H = 8.1r_c$, which is less than 1% lower than that for $q = 0.25$.

is increased. This leads to larger values of Schmidt number, which is a parameter that describes the ability of a fluid to transport momentum. In order to validate this model, we numerically calculated both the self-diffusion and the viscosity coefficients of a simple solution. The self-diffusion coefficient is calculated as

$$D_0 = \frac{1}{6Nt}\left\langle \sum_{i-1}^{N} |r_i(t_o + t) - r_i(t_o)|^2 \right\rangle \tag{14}$$

where N is the total number of particles and the brackets indicate an average over initial times, t_0. In Figure 1, the self-diffusion coefficient is shown as a function of the exponent q. This figure shows that the self-diffusion coefficient is reduced by a factor of 3.4, when the exponent q is decreased from 2 to 0.25.

In order to calculate the viscosity, the fluid is driven externally toward the positive direction of the x-axis via an applied uniform pressure gradient, dP/dx. As a result, a particle i experiences an external force

$$f_i = f_x x = -\frac{1}{\rho}\frac{\mathrm{d}P}{\mathrm{d}x}x \tag{15}$$

where ρ is the fluid number density. In Figure 2, the velocity profile is shown for $q = 0.25$, 0.5, 1 and 2 for a fluid driven by a force $f_x = 0.2\varepsilon/r_c$. This figure clearly demonstrates that the velocity field obeys the Poiseuille−Hagen law,[40]

$$v_f(z) = -\frac{1}{2\eta_0}\left|\frac{\mathrm{d}p}{\mathrm{d}x}\right|\left(z^2 - \frac{H^2}{4}\right) \tag{16}$$

Figure 2 also shows the interesting result that the effective position of the wall, $\pm$ H/2, determined from the intercept of the graph of $v_x^2(z)$ with the horizontal axis, increases with decreasing the exponent q (see inset of Figure 2). In Figure 3,

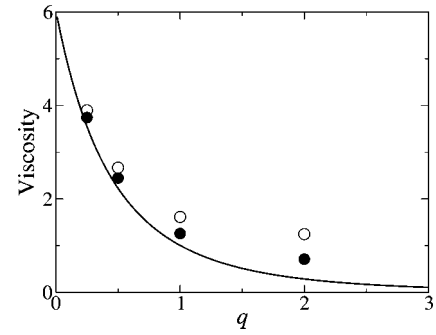

Figure 3. Solvent viscosity is shown vs the exponent q. The solid circles represent the full viscosity, η_0, and the open circles represent the contribution to the viscosity due to the dissipative forces, η_D. The solid line corresponds to the approximation given by eq 9 in ref 34.

Table 1. Values of the Diffusion Coefficient, Viscosity, and Schmidt Number, of a Simple DPD Fluid, as a Function of the Exponent q in Equation 13

q	$D_0[r_c^2/\tau]$	$\eta_0[\varepsilon\tau/r_c^3]$	Sc
0.25	0.0780	3.90	12.5
0.5	0.111	2.67	6.02
1	0.177	1.61	2.28
2	0.268	1.25	1.16

the fluid viscosity as extracted using eq 16 is shown. This figure indicates that the fluid viscosity is increased as the exponent q is decreased. These results are in accord with those obtained by Fan et al.[34]

The ability of a fluid to transport momentum is believed to be best described by Schmidt number, Sc, which is defined as the ratio between the speed of momentum diffusion and that of mass (particles) diffusion, i.e.,

$$Sc = \eta_0/m\rho D_0. \tag{17}$$

In a conventional DPD model, with $q = 2$, the Schmidt number $Sc \approx 1$, which is at least 2 orders of magnitude smaller than that of a typical fluid (e.g., the Schmidt number of water is about 500). In Table 1, the diffusivity, viscosity and Schmidt number of a simple DPD fluid are shown as a function of q. This table indicates that Schmidt number is increased by a factor of about 11 as q is decreased from 2 to 0.25. We verified that Sc is proportional to the square of the viscosity. This is expected since the diffusion coefficient $D_0 \sim 1/\eta_0$ and $Sc \sim \eta_0$. We note that a further increase in Sc for a given q can be achieved through increasing the cutoff of the dissipative force, $r_c^{(D)}$.[34] However, increasing $r_c^{(D)}$ is computationally very costly, since the number of interacting pairs is proportional to the cube of the cutoff distance. Therefore, in the present study, the effect of Schmidt number on the transport and migration properties of polymer solutions, is investigated through systematically varying the exponent q while keeping $r_c^{(D)} = r_c$.[41]

The simulations of Poiseuille flow were performed on boxes of dimensions $L_x \times L_y \times L_z$, with $L_x = L_y = 20r_c$, and $L_z = 2H + W_{wall}$ is the wall thickness, and $2H$ is the thickness of the slit. L_z is varied between $8r_c$ and $20r_c$. Due to the use of periodic boundary conditions along the three axes, the simulation box contains one wall only, parallel to the xy-plane. The fluid therefore interacts with both top and bottom sides of the wall. The fluid number density $\rho = 4r_c^{-3}$ and the temperature $k_BT = \varepsilon$ in most simulations, unless indicated. The polymer volume fraction is $\varphi = 0.06$. The random force parameter $\sigma = 3.0(\varepsilon^3 m/r_c^2)^{1/3}$. The wall is constructed from DPD particles which are arranged in a face-centered cubic lattice with a number density $61.35r_c^{-3}$. The high number density of the wall particles ensures that the solvent and polymer particles do not penetrate the wall. A time step $\Delta t = 0.005\tau$ where $\tau = (mr_c^2/\varepsilon)^{1/2}$ is used.

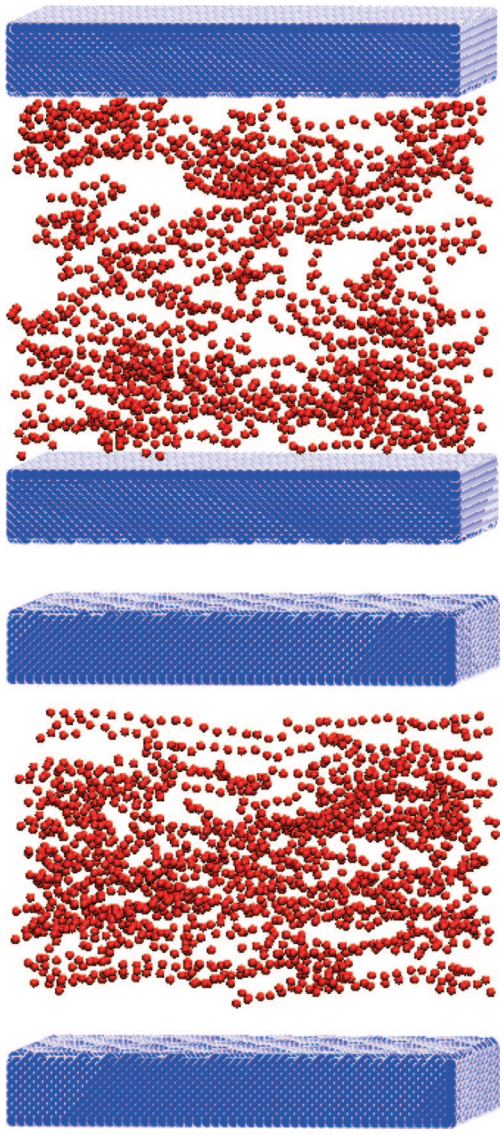

Figure 4. Snapshots of systems with $N = 20$ and $f_x = 0.4\varepsilon/r_c$. Top and bottom snapshots correspond to $q = 2$ and $q = 0.25$, respectively.

3. Results

To qualitatively demonstrate the effect of the exponent q on the distribution of the polymer chains in Poiseuille flow, steady-state snapshots of the polymers, with chain length $N = 20$ and driving force $f_x = 0.4\varepsilon/r_c$, are shown in Figure 4 for two different exponents corresponding to $q = 2$ and $q = 0.25$. This figure clearly demonstrates that the polymer chains are more depleted from the walls and more stretched along the flow direction for the case of $q = 0.25$ than for the case of $q = 2$.

In Figure 5, snapshots of the polymers with length $N = 20$ and exponent $q = 0.25$ are shown for the cases of $f_x = 0$ (equilibrium), $f_x = 0.2\varepsilon/r_x$ and $f_x = 0.4\varepsilon/r_c$. These snapshots show that the polymer chains become more stretched along the flow direction as the flow rate is increased. This is due to the increase in shear stresses as f_x is increased. Interestingly, these snapshots also show qualitatively that in this case, the polymers become more depleted from the walls vicinity as the flow rate is increased.

The flow strength is effectively described by a dimensionless number known as the Peclet number which is defined as the ratio between the rate of polymers advection and the rate of their diffusion, i.e.

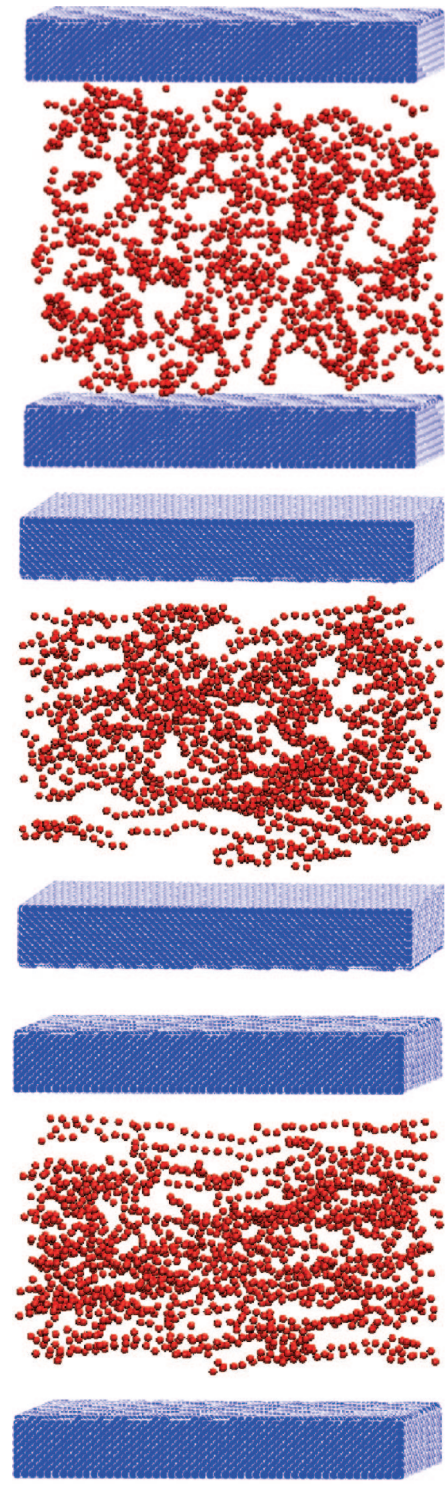

Figure 5. Snapshots of systems with $N = 20$ and $q = 0.25$. Snapshots from top to bottom correspond to $f_x = 0$ (equilibrium), $f_x = 0.2\varepsilon/r_c$, and $f_x = 0.4\varepsilon/r_c$, respectively.

$$Pe = \frac{\dot{\Gamma} R_g^{\,2}}{D_{CM}}, \tag{18}$$

where $\dot{\Gamma}$ is the mean shear rate, and in Poiseuille flow $\dot{\Gamma} \approx 2V_{max}/H$, R_g is the polymer chains radius of gyration at equilibrium, and D_{CM} is the diffusion coefficient of the polymers center-of-mass. In our simulations we found that in the dilute regime, the Peclet number is practically independent of the exponent q, and is proportional to the external force f_x. This is expected since both mean shear rate, $\dot{\Gamma}$ and D_{CM} are inversely

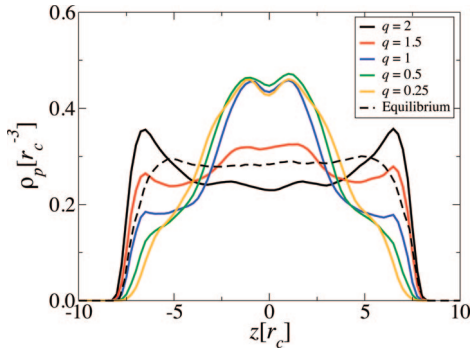

Figure 6. Polymer density profile for the case of $N = 20$ and $f_x = 0.4\varepsilon/r_c$. Data with solid lines from bottom to top at values of z close to the walls ($z = \pm 7r_c$) correspond to $q = 0.25$, 0.5, 1.0, 1.5 and 2.0, respectively. The dotted line corresponds to the system with $N = 20$ at equilibrium.

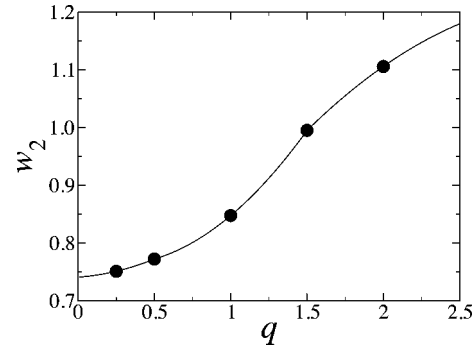

Figure 7. Second moment of the density profile, normalized by that at equilibrium, is shown as a function of the exponent q for the case of $N = 20$ and $f_x = 0.4\varepsilon/r_c$. The solid line is only a guide for the eye.

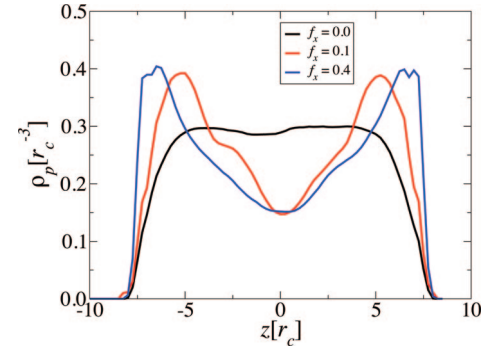

Figure 8. The polymer density profile for the case of $N = 100$ and exponent $q = 2$. Data lines from bottom to top at values of z close to the walls ($z = \pm 7r_c$) correspond to $f_x = 0.0$ ($Pe = 0$), $0.2\varepsilon/r_c$ ($Pe \approx 430$), and $0.4\varepsilon/r_c$ ($Pe \approx 860$), respectively.

proportional to the solvent viscosity, and the shear rate is proportional to the external force.

In Figure 6, the polymer mass distribution is shown for the case of $N = 20$, $f_x = 0.4\varepsilon/r_c$, and different values of the exponent corresponding to $q = 0.25$, 0.50, 1.0, 1.5, and 2.0. These systems are characterized by same Peclet number, $Pe \approx 120$ and a Wiessenberg number, $Wi = \dot{\Gamma}\eta_0 R_g^3/k_BT \approx 32$. Figure 6 shows that the presence of externally driven flow modifies the polymers mass distribution across the channel, when compared to their distribution at equilibrium which is uniform (shown by the dotted line). Figure 6 also shows that the polymers mass distribution in Poiseuille flow is affected by the exponent q, even though the Peclet number is practically unaffected by the value of q. For $q \geq 1.5$ and in the presence of flow, the depletion layer in vicinity of the wall is narrower than that at equilibrium. In contrast, for $q \leq 1$, the depletion layer in the presence of flow is larger than that at equilibrium, and is enhanced as q is further decreased. In the central region of the channel, there is a marked polymer depletion for the case of $q = 2$ when compared to the distribution at equilibrium. In contrast, when $q \leq 1.5$, the polymers volume fraction is enhanced in the central region of the channel. As reported in earlier studies.[15,25,29] We note that the DPD model accounts for the hydrodynamic interaction between polymer beads, as shown recently by us and others,[42,43] even in the case of $q = 2$. Therefore, the observed migration toward the channel walls in the case of $q = 2$ should be attributed to a suppression of the wall-polymer hydrodynamic interaction in the case of $q = 2$. The suppression of wall-polymer hydrodynamic interaction is due to the fact that wall-induced hydrodynamics is not developed enough during the flow time scale of the polymer chains in the case of low Schmidt number (e.g., for $q = 2$). The polymer distribution for $q = 2$ is similar to that observed in recent BDHI simulations by Jendrejack et al.,[15] when the wall-polymer hydrodynamic interaction is intentionally not accounted for. It is noted that although the overall shape of the polymers mass distributions obtained from the generalized DPD model in this work is in agreement with other models, the mass distribution exhibit interesting shoulders away from the centerline, which are particularly pronounced for $q = 1.5$ and $q = 1$. These shoulder mostly disappear, however, as q is further decreased. The physical origin of these shoulders is not understood at the moment, and require further investigation.

In the case of $q \leq 1.5$, the migration of the polymer chains toward the central region of the channel is in accord with experiments and with recent LBD, BDHI and MD simulations. We note that for $q \leq 1.5$, the polymer distributions are characterized by two off-center peaks separated by a shallow minimum. This feature was also observed in previous simulations. This nonmonotonic feature of the profile is attributed to the competition between the wall-polymer hydrodynamic interaction, which tends to drift the polymer chains away from the walls, and the cross-stream diffusion of the polymer chains, which is characterized by a nonuniform diffusivity due to their nonuniform conformational distribution across the channel.[31]

The cross-stream migration of the polymer chains is further examined through the second moment of the polymers mass distribution, normalized by its corresponding value at equilibrium,

$$W_2 = \left[\frac{\int_{-H2}^{H2} \mathrm{d}z\, z^2 \rho_p(z)}{\int_{-H2}^{H2} \mathrm{d}z\, z^2 \rho_p^{(0)}(z)}\right]^{1/2} \tag{19}$$

where $\rho_p^{(0)}$ is the polymer distribution at equilibrium. In Figure 7, the normalized second moment is shown vs q for systems with $N = 20$ and $f_x = 0.4\varepsilon/r_c$. A value $W_2 > 1$ implies a broadening of the polymers distribution as compared to that at equilibrium, and is therefore an indication of a cross-stream migration of the polymers toward the wall. Figure 6 shows that the depletion layer of the externally driven system with $q = 2$ is narrower than that at equilibrium, while the density is reduced in the middle of the channel. Although the case of $q = 1.5$ corresponds to $W_2 \approx 1$, the polymer distribution across the channel is nonuniform with a slight increase in polymer density close to the walls and a slight increase in the channel's centerline region. For $q < 1.5$, a clear cross-stream migration toward the channel's centerline is observed.

We now turn our attention to the effect of driving force on the cross-stream migration of the chains. In Figure 8 and Figure 9, the polymer density profiles for solutions containing polymers with $N = 100$ are shown for varying driving forces at $q = 2$

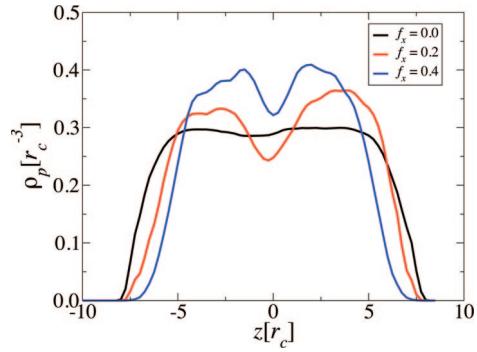

Figure 9. Polymer density profile for the case of $N = 100$ and exponent $q = 0.25$. Data lines from top to bottom at values of z close to the wall ($z = \pm 7r_c$) correspond to $f_x = 0.0$ ($Pe = 0$), $0.2\varepsilon/r_c$ ($Pe \approx 540$), and $0.4\varepsilon/r_c$ ($Pe \approx 1080$), respectively.

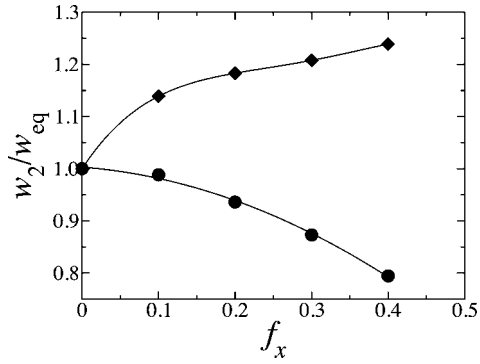

Figure 10. Second moment of the density profile as a function of the applied force f_x for the case of $N = 100$. Solid diamonds and solid bullets correspond to $q = 2$ and $q = 0.25$, respectively. The solid lines are guides for the eye.

and $q = 0.25$, respectively. These figures show that the direction of migration, as a function of external driving, is strongly affected by the value of the exponent q, and equivalently Schmidt number. In particular, for the case of high Schmidt number ($q = 0.25$), an increased polymer migration toward the centerline is observed with increasing the driving force (or equivalently Peclet number). In contrast, for the case of low Schmidt number ($q = 2$), an increased migration of the polymers toward the walls is observed with increasing Peclet number. In Figure 10, the corresponding normalized second moment, W_2, defined in eq 19 is shown for systems with $N = 100$, $q = 2$ and $q = 0.25$. This figure confirms the effect of the exponent q on the direction of migration. These results are in agreement with the proposal that the cross-stream migration of polymers is the result of interplay between the wall-polymer hydrodynamic interaction which tends to migrate the polymers away from the walls, and the Brownian motion of the polymers which tends to migrate the polymer chains toward the walls.

We now turn to the effect of chain length on the cross-stream migration of the polymer chains. In particular, we will focus on the case of high Schmidt number. In Figure 11, the polymer chains mass distribution for the case of $f_x = 0.2\varepsilon/r_c$ and $q = 0.25$ is shown for values of $N = 5$, 10, 15, 20, 50, and 100. This figure shows that for very short chains ($N = 5$ and $N = 10$), the polymer mass profile exhibits a single broad peak at the centerline. The double peak structure in the polymer mass distribution appears when $N \geq 15$. We attribute the lack of a double peak structure to the fact that the conformational anisotropy due to chain stretching is weak for short chains, thus leading to a practically uniform diffusion coefficient of the chains across the channel when N is low. Therefore, the driving force toward the walls, which is proportional to the gradient of

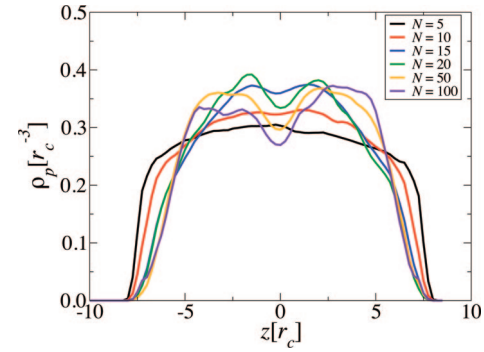

Figure 11. Polymer density profile for the case of $f_x = 0.2\varepsilon/r_c$ and $q = 0.25$. Chain length shown correspond to $N = 5$, 10, 15, 20, 50, and 100. The different chain lengths correspond to $Pe \approx 14$, 29, 47, 60, 147, and 280, for $N = 5$, 10, 15, 20, 50, and 100, respectively.

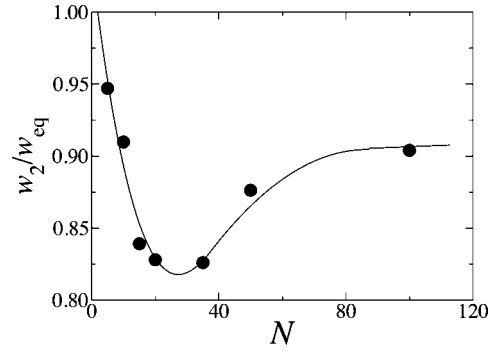

Figure 12. Second moment of the density profile, normalized by that at equilibrium, as a function of chain length for the case $f_x = 0.2\varepsilon/r_c$ and $q = 0.25$. The solid line is just a guide for the eye.

the diffusivity, is weak for short chains, thus leading the wall-polymer hydrodynamic interaction to be the dominant driving force resulting in a single peak at the centerline. In contrast, the diffusivity of the chains becomes increasingly nonuniform, along the z-axis, as N is increased.

The normalized second moment is shown as a function of chain length in Figure 12 for the case of $f_x = 0.2\varepsilon/r_c$ and $q = 0.25$, corresponding to Figure 11. Figure 12 shows that for short chains, the extent of polymer migration toward the centerline is amplified as N is increased. The second moment then reaches a minimum at about $N = 30$, and then decreases with further increase of chain length. This is due to the increase in hydrodynamic screening with the increase in chain length. We note that the minimum of the reduced second moment occurs at $H/R_g \approx 6.5$, which is in fairly good agreement with the recent Lattice Boltzmann study of Usta et al.,[25] where it was found that the direction of migration is reversed toward the channel walls when $H/R_g > 5$.

We note that since the driving force is kept constant for the different values of chain length, the Peclet number increases with increasing N, since $D_{CM} \sim R_g^{-1}$, according to the Zimm model,[42] and $R_g \sim N^{0.59}$ in the dilute regime. The results in Figure 11 and Figure 12 are in agreement with those obtained by Usta et al.[25] from Lattice Boltzmann simulations, where it is observed that the rate of increase of the degree of migration with increasing Peclet number is reduced with increasing chain length.

We also investigated the effect of slit thickness on the polymer density profile across the channel. We found that for high Schmidt number, $q = 0.25$, and chain length $N = 50$, the degree of migration away from the wall is accentuated as the thickness of the wall is increased. These results are again in good agreement with those obtained by Usta et al.[25] The

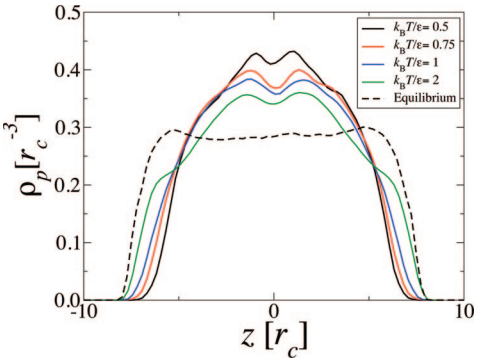

Figure 13. Effect of temperature on the polymer density profile for the case of $N = 20$, $q = 0.25$, and $f_x = 0.2\varepsilon/r_c$. Curves from top to bottom around $z = 0$ correspond to $k_BT/\varepsilon = 0.5$, 0.75, 1 and 2, respectively. These correspond to $Pe \approx 115$, 78, 60 and 32, respectively. The dashed line corresponds to the equilibrium density profile at $k_BT/\varepsilon = 2$. The equilibrium profile is weakly sensitive to temperature.

decrease in the degree of migration from the walls is due to the fact that the wall-induced hydrodynamic forces become increasingly screened by the closely separated walls. We also investigated the effect of temperature on the cross-stream migration. In Figure 13, the polymer density profiles is shown for systems with $N = 20$, $q = 0.25$, $f_x = 0.2\varepsilon/r_c$, and reduced temperature values corresponding to $k_BT/\varepsilon = 0.5$, 1.0, 1.5, and 2.0. This figure shows clearly that for a given driving force, the extent of the cross-stream migration of the polymers toward te central region of the channel is reduced with increasing temperature. We note that the Peclet number is almost constant for these systems. The reduction in the extent of migration toward the channel centerline, with increasing temperature, is attributed to the increase in Brownian diffusion of the polymer chains which tend to migrate the polymers toward the walls.

4. Summary and Conclusions

In this paper, we presented results of a computational study of dilute polymer solutions in nanoscale channels undergoing Poiseuille flow. The simulations use a generalized dissipative particle dynamics (DPD) approach, recently proposed by Fan et al.[34] Through varying the functional form of the weight function in the dissipative and random forces, this model allows for increasing Schmidt number, and therefore to better describe the transport properties of fluids. We investigated the effect of increasing Schmidt number on the trend of cross-stream migration of the polymer chains. Our central result is that when the Schmidt number is relatively low (∼1), as is the case in conventional DPD, a migration of the polymer chains toward the walls is observed. The degree of migration toward the walls is amplified as the external driving force is increased. In contrast, when the Schmidt number is increased (up to about 11), a net polymer cross-stream migration toward the channel centerline is observed. The degree of polymer migration away from the walls is amplified as the external driving force is increased. Although conventional DPD is able to well describe bulk hydrodynamic interactions in a polymer solution,[42] conventional DPD does not fully account for the wall−polymer hydrodynamic interaction believed to be the driving force of cross-stream migration away from the wall. In contrast generalized DPD with high Schmidt number does account for the wall-polymer hydrodynamic interaction leading to a cross-stream migration toward the channel centerline.

We also investigated the effects of chain length, channel width and temperature on the cross stream migration. We found that for short polymer chains and high Schmidt number, the extent of polymer cross-stream migration away from the wall is amplified as chain length is increased. This is due to the increase in wall−polymer hydrodynamic interaction with increasing chain length. However, as the chain length is further increased, the extent of polymer migration is reduced. This is due to an increase in screening of the hydrodynamic interaction resulting as the chain length is increased. For a given chain length and high Schmidt number, we found that the extent of cross-stream polymer migration away from the walls is decreased as the slit thickness is decreased. This is due to the increased closeness of the two walls, leading to screening of the wall−polymer hydrodynamic interaction. Finally, we found that the degree of migration away from the walls is reduced as temperature is increased, presumably due to the increase in cross-stream Brownian motion of the polymer chains. Although the results presented in this paper compare well with those obtained using BDHI and LBD, a quantitative comparison with these methods and experiments will be very useful, and is currently underway.

Acknowledgment. This work was supported by a grant from the Petroleum Research Fund of the American Chemical Society (42219-B7) and a grant from The University of Memphis Faculty Research Grant Fund. The latter support does not necessarily imply the endorsement by the University of research conclusions. Simulations were performed on computers at the University of Memphis High Performance Computing Facility. MEMPHYS is supported by the Danish National Research Foundation.

References and Notes

(1) Squires, T. M.; Quaqe, S. R. *Rev. Mod. Phys.* **2005**, *77*, 977.
(2) Wall, F. T.; Seitz, W. A.; Chin, J. C.; de Gennes, P. G. *PNAS USA* **1978**, *75*, 2069.
(3) Brochard, F.; de Gennes, P. G. *J. Chem. Phys.* **1977**, *67*, 52.
(4) Chen, Y.-L.; Graham, M. D.; Randall, G. C.; Gupta, M.; Doyle, P. S.; de Pablo, J. J. *Phys. Rev. E* **2004**, *70*, 06091.
(5) Balducci, A.; Mao, P.; Han, J. Y.; Doyle, P. S. *Macromolecules* **2006**, *39*, 6273.
(6) Izmitli, A.; Schwartz, D. C.; Graham, M. D.; de Pablo, J. J. *J. Chem. Phys.* **2008**, *128*, 085102.
(7) Agarwal, U. S.; Dutta, A.; Mashelkar, R. A. *Chem. Eng. Sci.* **1994**, *49*, 1693.
(8) Perkins, T. T.; Smith, D. E.; Chu, S. *Science* **1997**, *276*, 2016.
(9) Smith, D. E.; Chu, S. *Science* **1998**, *281*, 1335.
(10) Smith, D. E.; Babcock, H. P.; Chu, S. *Science* **1999**, *283*, 1724.
(11) Larson, R. G. *J. Rheol.* **2005**, *49*, 1.
(12) Fang, L.; Hu, H.; G Larson, R. *J. Rheol.* **2005**, *49*, 127.
(13) Stein, D.; van der Heydwn, F. H. J.; Koopans, W. J. A.; Dekker, C. *PNAS* **2006**, *103*, 15853.
(14) Jhon, M. S.; Freed, K. F. *J. Polym. Sci.: Polym. Phys.* **1985**, *23*, 955.
(15) Jendrejack, R. M.; Schwartz, D. C.; de Pablo, J. J.; Graham, M. D. *J. Chem. Phys.* **2004**, *120*, 2513.
(16) Ma, H.; Graham, M. D. *J. Chem. Phys.* **2005**, *17*, 083103.
(17) Jendrejack, R. M.; Graham, M. D.; de Pablo, J. J. *J. Chem. Phys.* **2000**, *113*, 2894.
(18) Jendrejack, R. M.; de Pablo, J. J.; Graham, M. D. *J. Chem. Phys.* **2002**, *116*, 7752.
(19) Woo, N. J.; Shaqfeh, E. S. G.; Khomami, B. *J. Rheol.* **2004**, *48*, 299.
(20) Jendrejack, R. M.; Dimalanta, E. T.; Schwartz, D. C.; Graham, M. D.; de Pablo, J. J. *Phys. Rev. Lett.* **2003**, *91*, 038102.
(21) Jendrejack, R. M.; de Pablo, J. J.; Graham, M. D. *J. Chem. Phys.* **2003**, *119*, 1164.
(22) Chen, Y.-L.; Graham, M. D.; de Pablo, J. J.; Jo, K.; Schwartz, D. C. *Macromolecules* **2005**, *38*, 6680.
(23) Hernández-Ortiz, J. P.; de Pablo, J. J.; Graham, M. D. *Phys. Rev. Lett.* **2007**, *98*, 140602.
(24) Usta, O. B.; Ladd, A. J. C.; Buttler, J. E. *J. Chem. Phys.* **2005**, *122*, 094902.
(25) Usta, O. B.; Buttler, J. E.; Ladd, A. J. C. *Phys. Fluids* **2006**, *18*, 031703.
(26) Usta, O. B.; Buttler, J. E.; Ladd, A. J. C. *Phys. Rev. Lett.* **2007**, *98*, 098301.
(27) Buttler, J. E.; Usta, O. B.; Kekre, R.; Ladd, A. J. C. *Phys. Fluids* **2007**, *19*, 113101.
(28) Chen, Y.-L.; Ma, H.; Graham, M. D.; de Pablo, J. J. *Macromolecules* **2007**, *40*, 5978.
(29) Khare, R.; Graham, M. D.; de Pablo, J. J. *Phys. Rev. Lett.* **2006**, *96*, 224505.
(30) Fan, X.; Phan-Thien, N.; Yong, N. T.; Wu, X.; Xu, D. *Phys. Fluids* **2003**, *15*, 11.

(31) Millan, J. A.; Laradji, M.; Wang, J. *J. Chem. Phys.* **2007**, *126*, 124905.
(32) Fedosov, D. A.; Karniadakis, G. E.; Caswell, B. *J. Chem. Phys.* **2008**, *128*, 144903.
(33) Groot, R. D.; Warren, P. B. *J. Chem. Phys.* **1997**, *107*, 4423.
(34) Fan, X.; Phan-Thien, N.; Chen, S.; Wu, X.; Ng, T. Y. *Phys. Fluids* **2006**, *18*, 063102.
(35) Hoogerbrugge, P. J.; Koelman, J. M. V. A. *Europhys. Lett.* **1992**, *19*, 155.
(36) Espanol, P.; Warren, P. *Europhys. Lett.* **1995**, *30*, 191.
(37) Espanol, P. *Europhys. Lett.* **1997**, *40*, 631.
(38) Pagonabarraga, I.; Hagen, M. H. J.; Frenkel, D. *Europhys. Lett.* **1998**, *42*, 377.
(39) Ripoll, M.; Ernst, M. H.; Espanol, P. *J. Chem. Phys.* **2001**, *115*, 7271.
(40) Landau, L. D. and Lifshitz, L. D., *Fluid Mechanics* (Pergamon Press, Oxford, 1987).
(41) We note that the Schmidt number can also be defined as the ratio between the polymers m momentum diffusion and their mass diffusion. We have calculated the diffusivity for a system containing a single chain with $N = 20$, and found that $D_{CM} \approx 0.015 r_c^2/\tau$ and $0.012 r_c^2/\tau$ for $q = 2$ and $q = 0.25$, respectively. This implies that the polymer Schmidt number, defined as $Sc = \eta_0/m\rho D_{CM}$, is 21 and 81 for $q = 2$ and $q = 0.25$, respectively. Therefore, the polymer Schmidt number though depends on the parameter q, is less sensitive to q when compared to the solvent Schmidt number.
(42) Jiang, W.; Huang, J.; Wang, Y.; Laradji, M. *J. Chem. Phys.* **2007**, *126*, 044901.
(43) Litvinov, S.; Ellero, M.; Hu, X.; Adams, N. A. *Phys. Rev. E* **2008**, *77*, 066703.

MA8014382